Journal of the Optical Society of America B
OPTICAL PHYSICS

Selecting plasmonic nanoshells for colorimetric sensors

RAPHAEL M. S. M. BALTAR,[1,2] SAJID FAROOQ,[1,3] AND RENATO E. DE ARAUJO[1,*]

[1]Laboratory of Biomedical Optics and Imaging, Federal University of Pernambuco, Brazil
[2]Federal Institute of Education, Science and Technology of Maranhão—IFMA, Brazil
[3]Center for Lasers and Applications, Instituto de Pesquisas Energeticas e Nucleares, IPEN—CNEN, Brazil
*renato.earaujo@ufpe.br

Received 1 November 2022; revised 12 January 2023; accepted 19 January 2023; posted 20 January 2023; published 27 February 2023

In this work, the use of gold and silver nanoshells was evaluated as a starting point for the establishment of colorimetric sensor platforms. The sensitivity and linearity of the nanoplatforms (SiO_2 core–metallic shell nanoparticles) were assessed under the influence of the nanoshell configuration, color space, and light source illuminant. A computational procedure for selecting high-performance plasmonic colorimetric sensor platforms is described. The evaluation methodology involves considering five different color spaces and 15 different color components. By exploring crucial figures of merit for sensing, the performance of the plasmonic nanoplatforms was evaluated, exploring Mie theory. We determined that gold nanoshells are highly efficient on colorimetric sensing, while silver nanoshells are a better choice for spectroscopic sensors. Plasmonic nanoplatforms based on nanoshells with 10 nm SiO_2 core radii and 5 nm thick Au shells presented sensitivity values up to 4.70 RIU^{-1}, considering the hue angle of the HSV color space. Color variation of up to 40% was observed, due to the adsorption of a 10 nm thick molecular layer on the gold nanoshell surface. In the search for advances in colorimetric biosensors, the optimization approach used in this work can be extended to different nanostructures.

https://doi.org/10.1364/JOSAB.479446

1. INTRODUCTION

Metallic nanostructures are important starting points for the development of optical sensor platforms. The interaction of light with metallic nanostrucutres may lead to a phenomenon known as localized surface plasmon resonance (LSPR), governed by the collective coherent oscillations of free electrons. The LSPR spectrum is reliant on shape, size, material of the nanoparticle (NP), and the surrounding dielectric medium refractive index (RI) [1].

In principle, LSPR can be achieved in any metal by fulfilling the Fröhlich condition: $\epsilon_r = -2\epsilon_m$ [2], where ϵ_r and ϵ_m are the real part of the NP and its surrounding non-absorbing medium, respectively. In particular, gold (Au) and silver (Ag) are the most used metals, with negative real dielectric values, on LSPR applications [3].

Plasmonic sensors are found in a wide variety of medical, biological, and chemical applications. In general, LSPR sensors stand on the identification of spectroscopic changes of plasmonic platform optical properties (transmittance or reflectance), which are induced by modification of the environment RI or immobilization of target molecules onto the sensor surface.

Plasmonic sensor behavior is highly dependent on the particle size and shape. Recently, Farooq *et al*. established a comprehensive approach to identify/optimize NP configurations for high-performance RI and molecular sensing [3].

The quantification of LSPR sensor performance is most commonly described in terms of bulk sensitivity (η_b), defined as the variation in the LSPR peak wavelength as a function of the RI of the medium, as [3]

$$\eta_b = \frac{\Delta\lambda_{\mathrm{LSPR}}}{\Delta n_m}, \tag{1}$$

where $\Delta\lambda_{\mathrm{LSPR}}$ is the wavelength shift of the LSPR peak, and Δn_m is the change in the RI of the surrounding medium.

The identification of the resonance peak shift can be masked by a broad LSPR spectrum. Therefore, the figure of merit (FoM) is defined as the ratio of bulk sensitivity to the full width at half-maximum (FWHM) [3]:

$$\mathrm{FoM} = \frac{\eta_b}{\mathrm{FWHM}}. \tag{2}$$

For molecular sensing, the immobilization of a target molecule on the NP surface can lead to the formation of a self-assembled monolayer (SAM) [4], which is characterized by an effective RI, given by [5]

$$n_{\mathrm{eff}} = (n_{\mathrm{ads}} - n_m)\left[1 - e^{-\left(\frac{2d_{\mathrm{ads}}}{l_d}\right)}\right], \tag{3}$$

where n_{ads} and n_m are the refractive indices of the adsorbed layer and surrounding medium, respectively. In Eq. (3), d_{ads} is the thickness of the adsorbed layer, and l_d is the decay length of the LSPR enhanced electromagnetic field. The identification of the effective RI allows to infer the wavelength shift of the sensing platform LSPR peak.

Several examples of plasmonic sensors and biosensors have been described in the literature, revealing that spherical NP-based platforms show high bulk sensitivity [6]. By exploring Ag nanospheres adhered on a glass slide and functionalized with monoclonal anti-Candida antibodies, Farooq *et al*. demonstrated the identification of a Candida albicans antigen [7]. LSPR molecular sensing based on Au nanospheres was also studied for dengue diagnosis in the acute phase of infection [8,9]. Based on the identification of η_b, FoM, and n_{eff}, Farooq *et al*. determined that a nanoshell (NS) composed of a SiO_2 core radius of 40 nm and a Au shell of 5 nm presents a high performance for biosensing purposes [3]. SiO_2/Au core–shell nanoplatforms can reach sensitivity values about 4x higher than massive Au nanospheres. Furthermore, a LSPR peak of AuNSs can be tunable from red to infrared by changing the shell thickness or radius, while AgNSs allow the establishment of plasmonic peaks at the visible spectrum. Complex nanostrucutures, such as nanocones or nanodimers [10], could also be explored as nanoplatforms for sensors. However, their manufacturing/assembling methods may limit the production of nanoplatforms and their widespread use.

The spectral analysis of LSPR nanoplatforms requires the use of instrumentation resources, such as spectrometers, which may restrain the use of plasmonic sensors in low-resource environments. However, plasmonic sensing platforms can also be developed to be explored with a naked-eye approach, in which LSPR peak variation allows visual identification of RI changes or molecular binding events. For instance, Khani *et al.* demonstrated a simple and sensitive colorimetric assay for naked-eye detection of mercury ions in water based on AuNP-catalyzed clock reaction [11]. Bastami *et al.* reported a novel and facile colorimetric assay based on Ag citrate-coated NPs as a chemosensor for the naked-eye detection of morphine. The developed optical sensing approach relied on the aggregation of Au-Ag NPs upon exposure to morphine, which led to an evident color variation from light yellow to brown [12]. Bakhori *et al.* presented an approach for ultrasensitive and affordable naked-eye detection and diagnosis of tuberculosis by utilizing a plasmonic enzyme-linked immunosorbent assay (ELISA) via antibody–antigen interaction [13]. More recently, Moitra *et al.* reported the development of a colorimetric assay based on AuNPs that could be used for diagnosing positive COVID-19 cases within 10 min from isolated RNA samples. AuNPs agglomerate selectively in the presence of the target RNA sequence of SARS-CoV-2 and demonstrate a change in surface plasmon resonance, resulting in a visual naked-eye detection of COVID-19 causative virus, SARS-CoV-2, without the requirement of any sophisticated instrumental techniques [14].

LSPR colorimetric sensors may exploit "aggregation" or "non-aggregation" detection strategies [15]. In general, solution-based platforms that use a NP aggregation approach show high sensitivity for chemical or molecular identification. NP aggregation induces significant shifts in the LSPR peak of the colloidal platform, which can be clearly identified by the naked eye. However, colloidal NP stability may restrict the use of solution-based platforms. Alternatively, the use of surface-based platforms, exploring a non-aggregation strategy, is considered as a robust approach for the development of LSPR sensors [15].

Notwithstanding the fact that the high subjectivity inherent to naked-eye analysis limits the reliability, repeatability, and sensitivity of the method, this approach is still of great importance and well described in the literature [16–18]. Nonetheless, applying imaging acquisition and processing introduces robustness to colorimetric evaluations. For instance, Wang *et al*. demonstrated a colorimetric biochemical sensor based on the use of plasmonic nanoarrays and a smartphone [19]. The colorimetric system evaluated the green component intensity of the image (in RGB color space) to measure protein concentration in urine samples. Toma and Tawa explored a colorimetric plasmonic platform to identify DNA hybridization by measuring hue angle changes in HSV color space [20].

Recently, Reinhard *et al*. described a methodology for optimizing nanosphere sizes for colorimetric sensors [21]. For that, colorimetric sensitivity, η_c, was defined as the ratio of the color space coordinate changes as a function of the medium RI variation. Therefore, η_c is given by

$$\eta_c = \frac{\Delta y}{\Delta n_m}, \tag{4}$$

where Δy is the intensity variation of a given color component, y, induced by a medium RI change, Δn_m. In addition, in [21], a detailed comparative analysis of the designed nanoplatform colorimetric sensitivity in five different color spaces was performed. It was found that Au nanospheres could lead to η_c values up to 1.4 RIU^{-1}, based on variation of hue angle values in HSV color space caused by the medium RI change. However, some fundamental aspects of plasmonic colorimetry were not fully explored in [21], such as the influence of the light source and shape of the nanostructure.

In this work, we extend the colorimetric sensor design methodology, exploiting different light sources. Moreover, SiO_2 core–metallic shell NPs are explored as a starting point for the establishment of an optical sensor platform. In addition, the evaluation methodology considers five different color spaces and 15 different color components, and the influence of NS geometric properties, material (Au and Ag), and light sources on sensor linearity and sensitivity. The robust analysis leads to the identification of optimized NSs for colorimetric sensor platforms.

2. METHODOLOGY

Here, NSs are considered to have a dielectric (SiO_2) core covered by a thin metallic (Au or Ag) layer. The strong coupling between charges in the inner and outer regions of the noble shell is responsible for the observed enhancement of the NP optical extinction. Combined with their outstanding optoelectronic properties, Au or Ag NSs exhibit excellent electrochemical properties, high electrical conductivity, and stability [22].

In this work, the absorption, scattering, and extinction cross sections (θ_{abs}, θ_{sca}, and θ_{ext}, respectively) of NSs were obtained

using the computational package PyMieScatt [23]. Considering nanostructures that are feasible to manufacture and with LSPR peaks in the visible spectrum, the NS core radius was varied from 10 to 50 nm and the shell thickness from 5 to 35 nm, for both spectroscopic and colorimetric analysis. The permissiveness values of Ag and Au were obtained from Johnson and Christy reported results [24]. The computational procedure was validated by comparing its findings with the NS spectroscopic results described in the literature.

The colorimetric evaluation considers that light is transmitted through a NS-based platform, with the absorbance peak normalized to 0.4 for all NS configurations, as in [21]. Exploring the Beer–Lambert law, the platform transmission spectrum was scaled by the standard color matching functions ($\mathrm{CIE}\bar{x}$, $\mathrm{CIE}\bar{x}$, $\mathrm{CIE}\bar{z}$), defined by the International Commission on Illumination (CIE) [25], and integrated across the visible wavelength range (360–830 nm). The obtained values were then normalized to the unattenuated CIE Y value, leading to CIE X, Y, and Z tristimulus values, described as [21]

$$X = \frac{\int_{360}^{830} \mathrm{CIE}\bar{x}(\lambda) \times \mathrm{illuminant}(\lambda) \times 10^{-A(\lambda)} \mathrm{d}\lambda}{\int_{360}^{830} \mathrm{CIE}\bar{y}(\lambda) \times \mathrm{illuminant}(\lambda)\, \mathrm{d}\lambda},$$

$$Y = \frac{\int_{360}^{830} \mathrm{CIE}\bar{y}(\lambda) \times \mathrm{illuminant}(\lambda) \times 10^{-A(\lambda)} \mathrm{d}\lambda}{\int_{360}^{830} \mathrm{CIE}\bar{y}(\lambda) \times \mathrm{illuminant}(\lambda)\, \mathrm{d}\lambda},$$

$$Z = \frac{\int_{360}^{830} \mathrm{CIE}\bar{z}(\lambda) \times \mathrm{illuminant}(\lambda) \times 10^{-A(\lambda)} \mathrm{d}\lambda}{\int_{360}^{830} \mathrm{CIE}\bar{y}(\lambda) \times \mathrm{illuminant}(\lambda)\, \mathrm{d}\lambda}, \quad (5)$$

where illuminant(λ) is the light source spectrum, and A is the sensor platform absorbance spectrum, which is proportional to σ_{ext}.

The tristimulus values provide a standard reference that can be used to define the coordinates in any other color spaces. In this study, we compared the use of five different color spaces (sRGB, rgb, CIELAB, HSV, and CIEXYZ) on nanosensor sensitivity. Therefore, 15 color components (y) were evaluated for each illuminant employed. As the color of an object is highly dependent on the illuminant spectrum, the sensing performance of the nanoplatform was evaluated exploring typical indoor light sources (fluorescent and white LED lamp) as well as sunlight. These light sources are defined by CIE as the standard illuminants: D65 (average daylight in the northern hemisphere), FL2 (fluorescent lamp), and LED-B4 (white LED lamp).

The colorimetric sensitivity was considered for each color component, according Eq. (4). The defined variation range of the medium RI varied from 1.33 to 1.43. The optimization procedure for colorimetric nanosensors used in this work is adaptable to any RI range of interest.

The linearity behavior of the colorimetric sensitivity was also considered, by weighting the R-squared (R^2) of each color space component in respect to the surrounding medium RI changes. Here, only nanoplatforms with $R^2 \geq 0.96$ were considered suitable for sensing purposes.

LSPR molecular sensing considers the adsorption of a dielectric monolayer on the surface of a metallic particle, embedded in water. The RI index of the molecular layer around the NS was considered to be $n_{\mathrm{ads}} = 1.47$, which represents a typical biological RI. The formation of a SAM around the NS induces changes in the effective RI, Eq. (3), of the surrounding medium.

3. RESULTS AND DISCUSSION

For optimization of NS-based colorimetric sensors, it is essential to describe the influence of NP geometric characteristics on the LSPR spectrum behavior. As depicted in Fig. 1, the absorption, scattering, and extinction cross section spectra of the Au and Ag NSs were identified. Figure 1(a) shows the extinction, absorption, and scattering cross sections of the AuNS with a 10 nm radius and shell thickness of 5 nm, in water (RI = 1.33). The Au nanostructure presents a LSPR peak at approximately 580 nm and a narrow extinction spectrum, which is mainly governed by absorption. For plasmonic sensing purposes, the narrow extinction spectrum of a plasmonic nanoplatform could lead to a low FoM value [Eq. (2)]. Similarly, Fig. 1(b) shows the optical cross sections for a AgNS with 30 nm radius and shell thickness of 10 nm. A strong LSPR peak resonance is observed at the visible spectrum at approximately 560 nm. Due to its larger size compared with the AuNS, it presents a relatively broader extinction spectrum that is governed by scattering.

The cross-section spectrum of the NS is strongly influenced by the nanostructure core radius and shell thickness. Figure 2(a) shows the mean values of the LSPR peak wavelength, considering the SiO_2 core radius and the Au shell thickness raging from

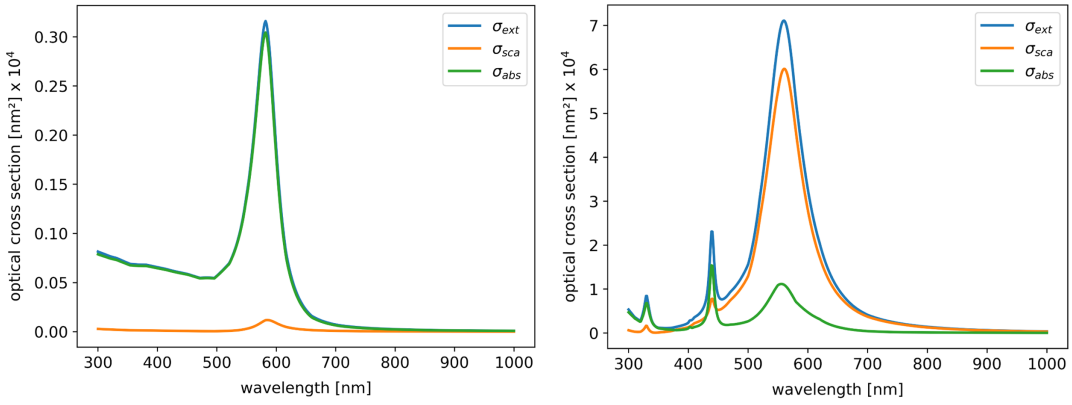

Fig. 1. Extinction, absorption, and scattering cross sections of (a) gold and (b) silver NSs in water.

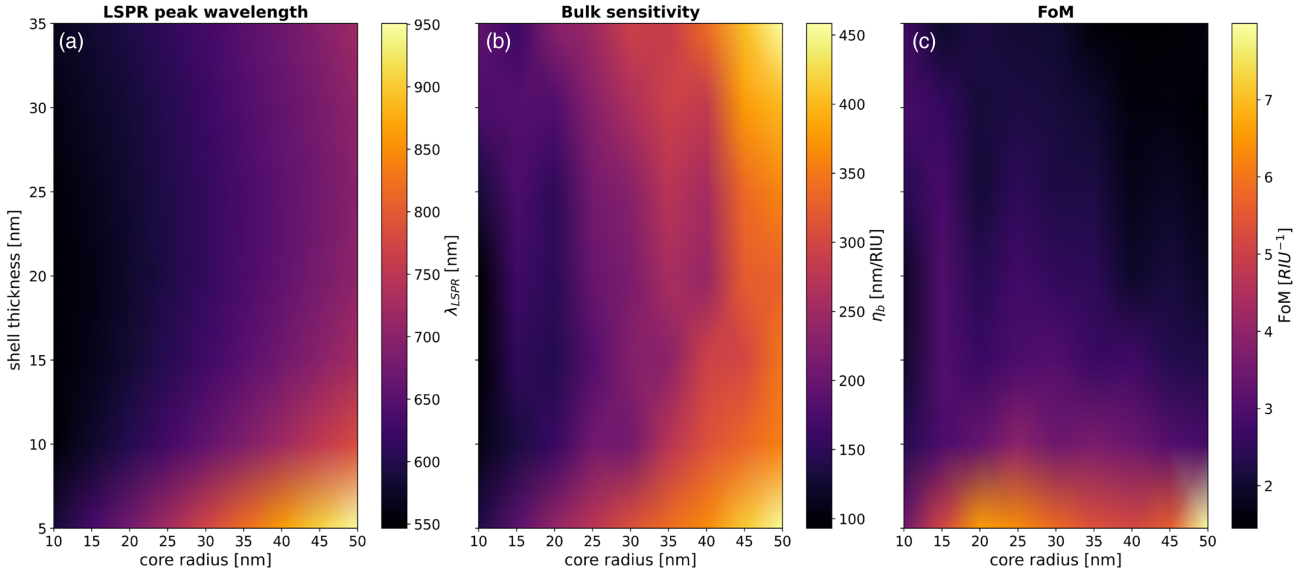

Fig. 2. Spectral analysis of the gold NS: (a) LSPR peak wavelength (RI = 1.33), (b) bulk sensitivity η_b, and (c) figure of merit FoM, considering RI values from 1.33 to 1.43.

10 to 50 nm and 5 to 35 nm, respectively. The NPs were considered to be in water (RI = 1.33). AuNS with a dielectric core radius smaller than 25 nm presents a LSPR peak at visible range, enabling colorimetric sensing. Particles with larger core radii (>30 nm) have LSPR peaks in the red–infrared spectral region, between 650 and 950 nm, which is attractive for biological applications in deep tissue regions.

The LSPR peak and FWHM were extracted from plasmonic spectra, considering the surrounding medium RI ranging from 1.33 to 1.43, which allows finding the bulk sensitivity [Eq. (1)] and FoM [Eq. (2)] for each nanoplatform. The η_b and FoM values of Au nanoplatforms are shown in Figs. 2(b) and 2(c), respectively. Figure 2(b) indicates that two NS configurations stand out with high bulk sensitivity values: the NS with 50 nm core radius and 5 nm shell thickness and the NS with 50 nm radius and 35 nm shell thickness.

The NS with 50 nm SiO_2 radius/35 nm Au thickness had the highest bulk sensitivity, $\eta_b = 450$ nm/RIU. However, its extinction spectrum is quite wide resulting in a low FoM, FoM = 1.66 RIU^{-1}. The AuNS with 50 nm SiO_2 radius/5 nm Au thickness exhibited the best overall result, with $\eta_b =$ 450 nm/RIU and FoM = 7.9 RIU^{-1}. Considering a AuNS sensor platform, Farooq *et al*. reported $\eta_b = 381$ nm/RIU and FoM = 5.4 RIU^{-1} for AuNS with 40 nm radius and 5 nm thickness [3].

In the case of AgNS, the LSPR peak is found in the visible spectrum region, for nanostructures with metallic shells thicker than 15 nm, as shown in Fig. 3(a). As depicted in Fig. 3(b), the

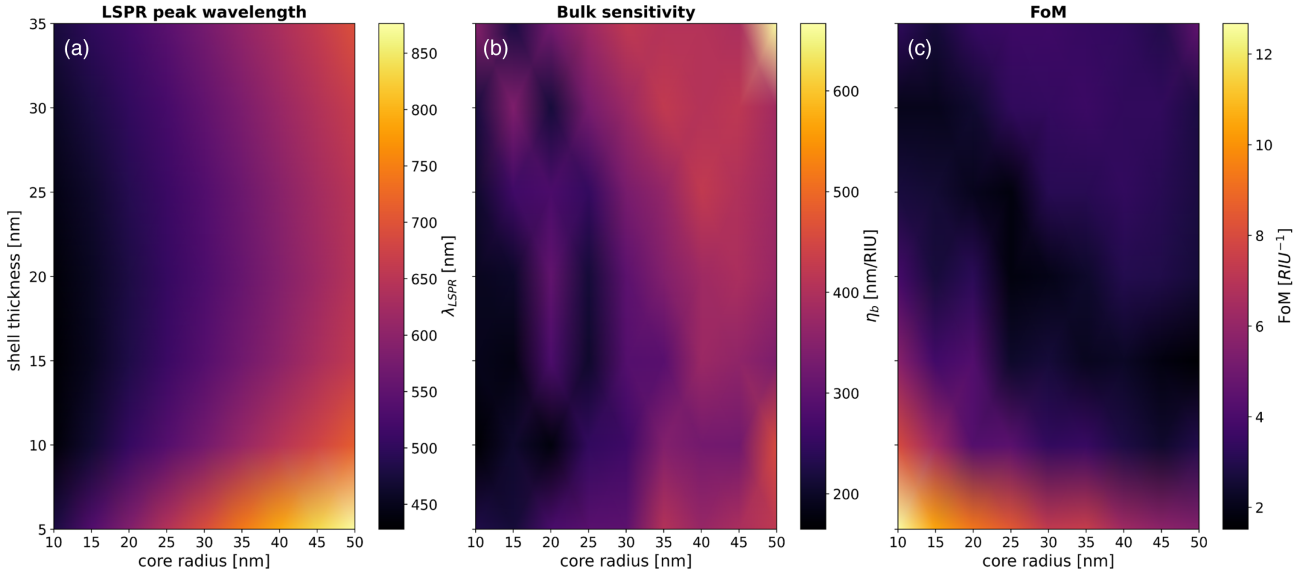

Fig. 3. Spectral analysis of the silver NS: (a) LSPR peak wavelength (RI = 1.33), (b) bulk sensitivity η_b, and (c) figure of merit FoM, considering RI values from 1.33 to 1.43.

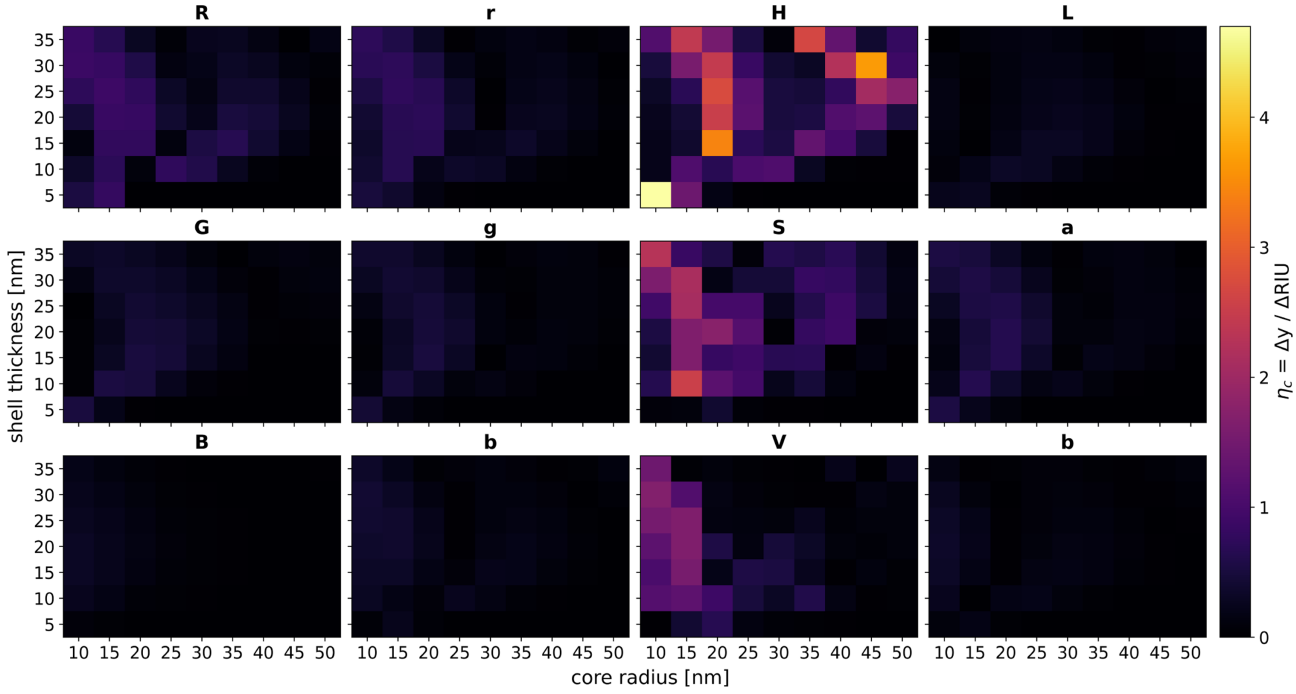

Fig. 4. Colorimetric sensitivity of AuNS with respect to radius and thickness variation, for the LED-B4 illuminant and RI ranging from 1.33 to 1.43.

highest bulk sensitivity value, $\eta_b = 664$ nm/RIU, was found for the nanostructure (50 nm radius/35 nm shell thicknesses). In general, NPs with large surface areas show high bulk sensitivity values, but low FoM values. The AgNS with radius of 10 nm and shell thickness of 5 nm had the highest FoM, FoM = 12.6 RIU^{-1}, as shown in Fig. 3(c).

For colorimetric sensing purposes, the nanoplatform should present LSPR peaks and high sensitivity and FoM values in the visible spectrum range. Therefore, optimized nanoplatforms for spectroscopic sensing may not be ideal for colorimetric technics.

As described in the methodology, the tristimulus values (X, Y, and Z) of the CIE XYZ color space were obtained from the extinction spectra of metallic NSs. From the tristimulus values, 12 other color parameters (R, G, and B; r, g, and b; H, S, and V; L, A, and B) from sRGB, rgb, HSV, and CIE LAB were obtained considering three different illuminants (D65, FL2, and LED-B4). Figure 4 shows the colorimetric sensitivity values [Eq. (4)] of AuNS subjected to LED-B4 illuminant.

Likewise, the sensitivity and linearity of the colorimetric Au nanoplatform were also studied considering FL2 and D65 illuminants. Table 1 presents a summary of AuNS configurations and color parameters with highest sensitivity and linearity values with respect to each analyzed illuminant. For AuNS, the highest sensitivity values were identified at the hue color parameter of HSV color space ($\eta_c = 4.70$ RIU^{-1}), found for NS with 10 nm radius and 5 nm Au shell thickness subjected to LED-B4 illuminant. Although NS with 5 nm Au thickness is not commercially available, the nanostructure can be synthesized [26].

Table 1. Identification of High Performance AuNS Sensing Platform Configuration for Different Illuminants and Color Spaces

Illuminant	Color Parameter	Radius (nm)	Thickness (nm)	η_c (RIU^{-1})	R^2
D65	Saturation	20	15	1.89	0.99
FL2	Value	15	5	1.83	0.99
LED-B4	Hue	10	5	4.70	0.97

The colorimetric sensitivity analysis of AgNS subjected to the FL2 illuminant is shown in Fig. 5. The highest sensitivity value ($\eta_c = 4.09$ RIU^{-1}) was found for the AgNS with 30 nm radius and 10 nm shell. In that case, the saturation color parameter of HSV color space is to be considered for high-performance colorimetric sensing. Table 2 summarizes the highest colorimetric sensitivity values found for the AgNS nanoplatform considering the analyzed color parameters and illuminants.

The literature indicates colorimetric sensors base on complex plasmonic structures, reaching sensitivity values lower than the ones described in Tables 1 and 2. Kim *et al*. developed a plasmonic nanohole array for biosensing applications that achieved a normalized sensitivity of $\eta_c = 0.5$ RIU^{-1}, analyzing the CIE LAB color space [27]. Wang *et al*. obtained a normalized sensitivity of $\eta_c = 2.28$ RIU^{-1} with a nanostructured plasmonic sensor based on nano Lycurgus cup arrays, in RGB color space [19]. Reinhard *et al*. obtained a colorimetric sensitivity of $\eta_c = 1.4$ RIU^{-1} for bare nanospheres with radii of approximately 91 nm (optimized structure), regarding a D65 illuminant and color component hue (HSV) [21]. Therefore, an improvement of 335% on colorimetric sensitivity is achieved by applying AuNS instead of nanospheres and by exploring the appropriate illuminant.

Optical cross sections of the identified optimal nanoplatforms for colorimetric sensing (AuNS with 10 nm radius and 5 nm shell and AgNS with 30 nm radius and 10 nm shell) are

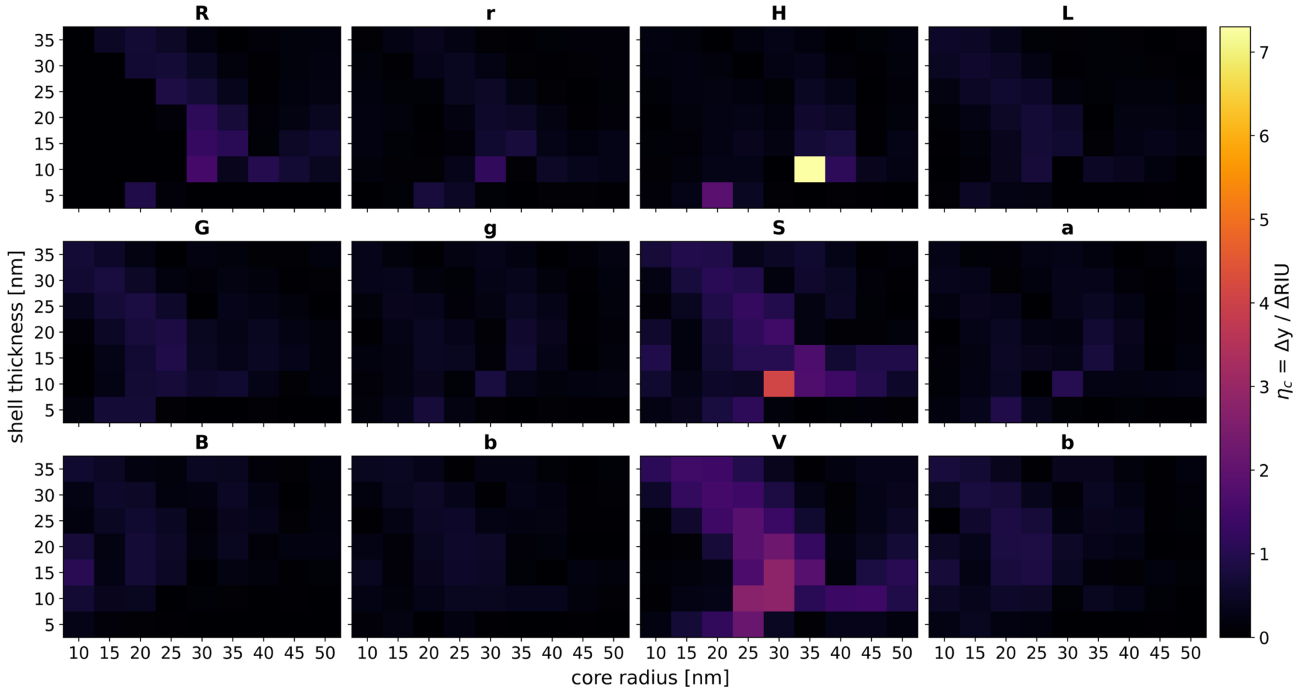

Fig. 5. Colorimetric sensitivity of AgNS with respect to radius and thickness variation, for the FL2 illuminant and RI range of 1.33 to 1.43.

Table 2. Identification of High Performance AgNS Sensing Platform Configuration for Different Illuminants and Color Spaces

Illuminant	Color Parameter	Radius (nm)	Thickness (nm)	η_c (RIU^{-1})	R^2
D65	Hue	35	25	2.69	0.98
FL2	Saturation	30	10	4.09	0.99
LED-B4	Saturation	35	15	3.05	0.99

shown in Fig. 1, with LSPR resonances at the visible electromagnetic spectral range. The optimized sensing platforms have $R^2 > 0.97$, as indicated in Tables 1 and 2. The color component variation with respect to surrounding medium RI variation for the identified best performance nanoplatforms is shown in Fig. 6, indicating the linear behavior of the nanosensor. Although the obtained values for η_c are smaller for AgNS than AuNS, the sensing platform based on AgNPs leads to better linear performance.

The nanoplatforms were evaluated for molecular sensing. LSPR biosensors are based on the adsorption of a target molecule on the surface of the metallic NP, changing the RI of the NP's surrounding medium. For specific molecular identification, recognition elements such as antigens, DNA, enzymes, or aptamers (with 1 to 6 nm typical spherical diameters) are used [28–30]. Short ligands such as cysteine and cysteamine (2 to 4 nm length) are also explored binding the recognition elements to the metallic surface [31]. Therefore, LSPR biosensor nanoplatforms have a recognition molecular monolayer with approximately 10 nm thickness.

Figure 7(a) shows the NS LSPR spectral peak shift as a function of the adsorbent molecular layer thickness. As AgNS presents a larger surface than AuNS, longer LSPR shifts can be induced on the AgNS spectrum, as compared to the AuNS spectrum. Figure 7(b) depicts the behavior of the hue intensity

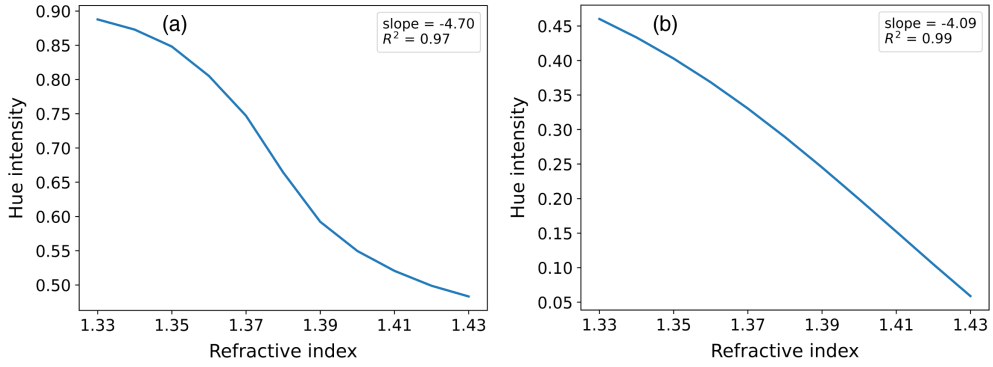

Fig. 6. Color component variation with respect to surrounding medium RI variation for (a) AuNS with 10 nm radius and 5 nm shell illuminated by LED-B4 and (b) AgNS with 30 nm radius and 10 nm shell illuminated by FL2.

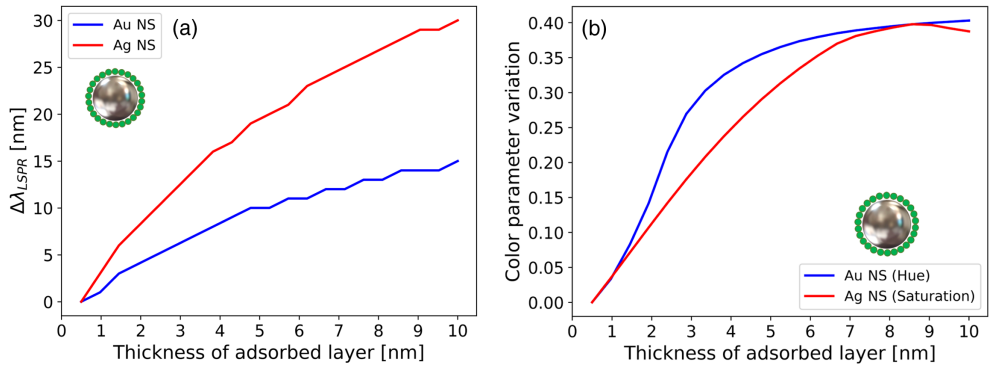

Fig. 7. Molecular sensing analysis with the adsorbent layer thickness varying from 0.5 to 10 nm for (a) LSPR spectral shift and (b) color component variation, hue for AuNS, and saturation for AgNS.

change for Au and Ag NSs. The adsorption of a 10 nm thick monolayer on the NS induces significant changes in color parameters ($\Delta y \approx 38\%$ for AgNS under FL2 illuminant and $\Delta y \approx 40\%$ for AuNS under LED-B4 illuminant).

One strategy to enhance the performance of plasmonic sensors is to explore surface-based platforms, where NPs are deposited on dry surfaces [3]. In that case, the sensor reading is done after drying the surface posterior to the establishment of the molecular layer.

4. CONCLUSION

The search for low-cost, label-free molecular biosensors has driven an increase in research in the field of plasmonics. The analysis of performance parameters (sensitivity and FoM) is imperative for the establishment of better nanosensors. The obtained computational results show promising NS configurations for spectroscopic sensors. The performance of NSs as spectroscopic sensing platforms is highly dependent on the particle material and structure (radius and shell thickness). Sensor platforms based on AgNS with 50 nm radius and 35 nm shell thickness stand out, with $\eta_b = 664$ nm/RIU. To the best of our knowledge, this is the highest bulk sensitivity value reported in the literature for LSPR sensors based on spherical structures. The spectroscopic analysis is independent of the illuminant due to the nature of the spectroscopic analyses.

For colorimetric sensors, the illuminant spectrum should also be considered. Moreover, different color spaces were explored on evaluation of colorimetric platforms. On the identification of high-performance NS colorimetric sensing platforms, the sensitivity and linearity of the nanoplatform were assessed. The AuNS with 10 nm radius and 5 nm shell thickness subjected to LED-B4 illuminant exhibited the highest colorimetric sensitivity ($\eta_c = 4.70\,\mathrm{RIU}^{-1}$) for the hue color parameter. The nonlinear behavior of the color parameters to medium RI changes limits the performance of the sensing platform. Color intensity (hue angle) variation of up to 40% was identified, due to the adsorption of a 10 nm thick molecular layer on the AuNS surface.

This work also reveals that optimized plasmonic platforms for spectroscopic sensing are not necessarily adequate for high performance colorimetric sensors. Moreover, the choice of the metallic shell (Au or Ag) for colorimetric sensors should consider the illuminant and the color space to be used.

Acknowledgment. The authors are grateful to Conselho Nacional de Desenvolvimento Científico e Tecnológico (CNPq), National Institute of Science and Technology of Photonics (INCT de Fotônica), and Coordenação de Aperfeiçoamento de Pessoal de Nível Superior (CAPES).

Disclosures. The authors declare no conflicts of interest.

Data availability. Data underlying the results presented in this paper are not publicly available at this time but may be obtained from the authors upon reasonable request.

REFERENCES

1. A. J. Haes, W. Paige Hall, L. Chang, W. L. Klein, and R. P. Van Duyne, "A localized surface plasmon resonance biosensor: first steps toward an assay for Alzheimer's disease," Nano Lett. **4**, 1029–1034 (2004).
2. E. Petryayeva and U. J. Krull, "Localized surface plasmon resonance: nanostructures, bioassays and biosensing–a review," Anal. Chim. Acta. **706**, 8–24 (2011).
3. S. Farooq, D. Rativa, and R. E. de Araujo, "Optimizing the sensing performance of SiO_2-Au nanoshells," Plasmonics **14**, 1519–1526 (2019).
4. M. D. Malinsky, K. L. Kelly, G. C. Schatz, and R. P. Van Duyne, "Chain length dependence and sensing capabilities of the localized surface plasmon resonance of silver nanoparticles chemically modified with alkanethiol self-assembled monolayers," J. Am. Chem. Soc. **123**, 1471–1482 (2001).
5. L. S. Jung, C. T. Campbell, T. M. Chinowsky, M. N. Mar, and S. S. Yee, "Quantitative interpretation of the response of surface plasmon resonance sensors to adsorbed films," Langmuir **14**, 5636–5648 (1998)
6. S. Farooq and R. E. de Araujo, "Engineering a localized surface plasmon resonance platform for molecular biosensing," Open J. Appl. Sci. **8**, 126–139 (2018).
7. S. Farooq, W. Neves, O. G. Pandoli, and T. Del Rosso, "Engineering a plasmonic sensing platform for candida albicans antigen identification," J. Nanophoton. **12**, 033003 (2018).
8. A. Camara, P. Gouvêa, A. Dias, A. Braga, R. Dutra, R. de Araujo, and I. Carvalho, "Dengue immunoassay with an LSPR fiber optic sensor," Opt. Express **21**, 27023–27031 (2013).
9. S. Farooq, F. Wali, D. M. Zezell, R. E. de Araujo, and D. Rativa, "Optimizing and quantifying gold nanospheres based on LSPR label-free biosensor for dengue diagnosis," Polymers (Basel) **14**, 1592 (2022).
10. S. Farooq, D. Rativa, Z. Said, and R. E. de Araujo, "Ultra-sensitive narrow-band plasmonic perfect absorber for sensing applications," Photon. Nanostr. Fundam. Appl. **50**, 101018 (2022).
11. H. Khani, S. Abbasi, M. T. Yaraki, and Y. N. Tan, "A naked-eye colorimetric assay for detection of Hg^{2+} ions in real water samples based

on gold nanoparticles-catalyzed clock reaction," J. Mol. Liq. **345**, 118243 (2022).
12. T. R. Bastami, M. Bayat, and R. Paolesse, "Naked-eye detection of morphine by Au@Ag nanoparticles-based colorimetric chemosensors," Sensors **22**, 2072 (2022).
13. N. M. Bakhori, N. A. Yusof, J. Abdullah, H. Wasoh, M. S. S. Noor, N. H. A. Raston, and F. Mohammad, "Immuno nanosensor for the ultrasensitive naked eye detection of tuberculosis," Sensors, **18**, 1932 (2018).
14. P. Moitra, M. Alafeef, K. Dighe, M. B. Frieman, and D. Pan, "Selective naked-eye detection of SARS-CoV-2 mediated by N gene targeted antisense oligonucleotide capped plasmonic nanoparticles," ACS Nano **14**, 7617–7627 (2020).
15. E. Mauriz, "Clinical applications of visual plasmonic colorimetric sensing," Sensors **20**, 6214 (2020).
16. Z. Zhang, H. Wang, Z. Chen, X. Wang, J. Choo, and L. Chen, "Plasmonic colorimetric sensors based on etching and growth of noble metal nanoparticles: strategies and applications," Biosens. Bioelectron. **114**, 52–65 (2018).
17. A. Orouji, S. Abbasi-Moayed, F. Ghasemi, and M. R. Hormozi-Nezhad, "A wide-range pH indicator based on colorimetric patterns of gold@silver nanorods," Sens. Actuators B Chem. **358**, 131479 (2022).
18. Z. Zhang, Z. Chen, S. Wang, F. Cheng, and L. Chen, "Iodine-mediated etching of gold nanorods for plasmonic elisa based on colorimetric detection of alkaline phosphatase," ACS Appl. Mater. Interfaces **7**, 27639–27645 (2015).
19. X. Wang, T. W. Chang, G. Lin, M. R. Gartia, and G. L. Liu, "Self referenced smartphone-based nanoplasmonic imaging platform for colorimetric biochemical sensing," Anal. Chem. **89**, 611–615 (2017).
20. M. Toma and K. Tawa, "Plasmonic coloration of silver nanodome arrays for a smartphone-based plasmonic biosensor," Nanoscale Adv. **1**, 3699–3708 (2019).
21. I. Reinhard, K. Miller, G. Diepenheim, K. Cantrell, and W. Paige Hall, "Nanoparticle design rules for colorimetric plasmonic sensors," ACS Appl. Nano Mater. **3**, 4342–4350 (2020).
22. K. S. Lee and M. A. El-Sayed, "Gold and silver nanoparticles in sensing and imaging: sensitivity of plasmon response to size, shape, and metal composition," J. Phys. Chem. B **110**, 19220–19225 (2006).
23. B. J. Sumlin, W. R. Heinson, and R. K. Chakrabarty, "Retrieving the aerosol complex refractive index using pymiescatt: a Mie computational package with visualization capabilities," J. Quant. Spectrosc. Radiat. Transfer **205**, 127–134 (2018).
24. P. B. Johnson and R. W. Christy, "Optical constants of the noble metals," Phys. Rev. B **6**, 4370–4379 (1972).
25. H. S. Fairman, M. H. Brill, and H. Hemmendinger, "How the CIE 1931 color-matching functions were derived from Wright-Guild data," Color Res. Appl. **22**, 11–23 (1997).
26. Y. Jin, C. Jia, S. W. Huang, M. O'Donnell, and X. Gao, "Multifunctional nanoparticles as coupled contrast agents," Nat. Commun. **1**, 41 (2010).
27. S. Kim, L. Youngjin, K. Y. Jae, Y. H. Jae, K. Hyuk-Jun, H. Y. Jae, M. Cheil, and J. E. Jae, "Color-sensitive and spectrometer-free plasmonic sensor for biosensing applications," Biosens. Bioelectron. **126**, 743–750 (2019).
28. M. A. Morales and J. M. Halpern, "Guide to selecting a biorecognition element for biosensors," Bioconjugate Chem. **29**, 3231–3239 (2018).
29. J. P. Chambers, B. P. Arulanandam, L. L. Matta, A. Weis, and J. J. Valdes, "Biosensor recognition elements," Current Issues Mol. Biol. **10**, 1–12 (2008).
30. H. P. Erickson, "Size and shape of protein molecules at the nanometer level determined by sedimentation, gel filtration, and electron microscopy," Biol Proced Online, **11**, 32 (2009).
31. S. Bayram, O. K. Zahra, and A. S. Blum, "Short ligands offer long-term water stability and plasmon tunability for silver nanoparticles," R Society Chem. Adv. **5**, 6553–6559 (2015).